Synchronization and Collective Dynamics in a Carpet of Microfluidic Rotors

Nariya Uchida[1,*] and Ramin Golestanian[2,†]

[1]Department of Physics, Tohoku University, Sendai, 980-8578, Japan
[2]Department of Physics and Astronomy, University of Sheffield, Sheffield S3 7RH, United Kingdom

(Received 12 November 2009; published 26 April 2010)

We study synchronization of an array of rotors on a substrate that are coupled by hydrodynamic interaction. Each rotor, which is modeled by an effective rigid body, is driven by an internal torque and exerts an active force on the surrounding fluid. The long-ranged nature of the hydrodynamic interaction between the rotors causes a rich pattern of dynamical behaviors including phase ordering and self-proliferating spiral waves. Our results suggest strategies for designing controllable microfluidic mixers using the emergent behavior of hydrodynamically coupled active components.

DOI: 10.1103/PhysRevLett.104.178103 PACS numbers: 87.19.rh, 07.10.Cm, 47.61.Ne, 87.80.Fe

Introduction.—Microorganisms and the mechanical components of the cell motility machinery such as cilia and flagella operate in low Reynolds number conditions where hydrodynamics is dominated by viscous forces [1]. The medium thus induces a long-ranged hydrodynamic interaction between these active objects, which could lead to emergent many-body behaviors. Examples of such cooperative dynamical effects include sperms beating in harmony [2], metachronal waves in cilia [3–5], formation of bound states between rotating microorganisms [6], and flocking behavior of red blood cells moving in a capillary [7]. For a collection of free swimmers, such as microorganisms [8], hydrodynamic interactions have been shown to lead to instabilities [9,10] that can result in complex dynamical behaviors [10,11]. In the context of simple microswimmer models where hydrodynamic interactions coupled to internal degrees of freedom can be studied with minimal complexity, it has been shown that the coupling could result in complex dynamical behaviors such as oscillatory bound states between two swimmers [12] and collective many-body swimming phases [13,14].

A particularly interesting aspect of such hydrodynamic coupling is the possibility of synchronization between different objects with cyclic motions [4,5,15–21]. This effect has mostly been studied in simple systems such as two interacting objects or linear arrays and very little is known about possible many-body emergent behaviors of a large number of active objects with hydrodynamic coupling. For example, in a recent experiment [22], Darnton *et al.* observed chaotic flow patterns with complex vortices above a carpet of bacteria with their heads attached to a substrate and their flagella free to interact with the fluid (see also [23]). On the other hand, recent advances from micron-scale magnetically actuated tails [24] to synthetic molecular rotors [25] now allow fabrication of arrays of active tails that can stir up the fluid. It is therefore very important to explore the possible complexity of the phase behavior of such an actively stirred microfluidic system.

Here, we consider a simple generic model of rotors [26] positioned on a regular 2D array on a substrate and study their collective dynamics numerically. We find that the long-ranged hydrodynamic interactions could either enhance or destroy ordering, depending on the degree of a built-in *geometric frustration* that originates from the interaction of the rotors with the fluid. More specifically, our model adopts a fully synchronized state when the frustration is weak, and a randomly disordered state when it is maximally frustrated. Moreover, the dynamics of the system leads to self-proliferating spiral waves between the above two limiting behaviors. We also take into account thermal fluctuations of the rotors and map out the phase diagram of the system as a function of temperature and the degree of frustration.

Model and dynamical equations.—We consider an array of rotors that are assumed to be spherical beads of radius a moving on circular trajectories of radius b, which are positioned on a rectangular lattice of base length d and at a height h above a substrate (see Fig. 1). The ith rotor is anchored at $\mathbf{r}_{i0}$ to the surface of the substrate, which we take to be the xy plane. The instantaneous position of the rotating bead is $\mathbf{r}_i = \mathbf{r}_{i0} + b\mathbf{n}_i + h\mathbf{e}_z$, where the unit vector $\mathbf{n}_i(t) = (\cos\phi_i(t), \sin\phi_i(t), 0)$ gives the orientation of the arm of the rotor. Because of the constraint that the bead is only allowed to move on the circular orbit of radius b, the

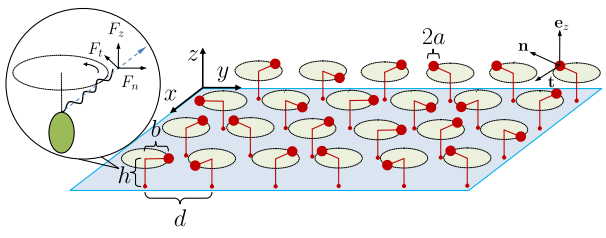

FIG. 1 (color online). Schematic representation of the array of rotors. Inset: an immobilized bacterium with active flagella as a possible realization of a rotor that can exert both a tangential drag and an active radial force on the fluid.

velocity of the rotor can be written as $\mathbf{v}_i = b\frac{d\mathbf{n}_i}{dt} = b\frac{d\phi_i}{dt}\mathbf{t}_i$, where $\mathbf{t}_i = \mathbf{e}_z \times \mathbf{n}_i = (-\sin\phi_i, \cos\phi_i, 0)$ is the unit vector tangent to the trajectory.

We assume that the structure of the rotor is such that it drags the fluid with it as it moves (tangentially) along the circular trajectory, while it can also pump the fluid radially due to some internal degrees of freedom. The inset of Fig. 1 shows a possible realization of such a system in the case of bacteria whose heads are fixed on the substrate. In this example, the spinning rotation of the flagella would produce the pumping effect, while the precession of the axis of the flagella about the anchoring point would correspond to the tangential motion of the bead. Therefore, in our simplified model, each rotor exerts a force, which can be decomposed into the radial, tangential, and vertical components as $\mathbf{F}_i = F_n\mathbf{n}_i + F_t\mathbf{t}_i + F_z\mathbf{e}_z$. The velocity field of the fluid created by the rotors is given by $\mathbf{v}(\mathbf{r}) = \sum_i \mathbf{G}(\mathbf{r} - \mathbf{r}_i)\cdot\mathbf{F}_i$ where $\mathbf{G}(\mathbf{r})$ is the Blake-Oseen tensor [27], which describes the hydrodynamic interaction near a flat surface with the nonslip boundary condition. Assuming that the arm length b and the height h are much smaller than the characteristic distance d between the rotors, we can use the $O(h^2/d^2)$ approximation [4], $G_{\alpha\beta}(\mathbf{r}) = \frac{3h^2}{2\pi\eta}\frac{r_\alpha r_\beta}{|\mathbf{r}|^5}$ for α, $\beta = x$, y, and $G_{\alpha z}(\mathbf{r}) = G_{z\alpha}(\mathbf{r}) = G_{zz}(\mathbf{r}) = 0$, for $\alpha = x$, y. Note that the z component of the force is not coupled to flow and that the fluid velocity is lying in the xy plane.

To obtain the flow velocity at the position of the rotors, we need to subtract the self-interaction, which involves the Stokes drag coefficient $\zeta = 6\pi\eta a$. This yields

$$\frac{d\phi_i}{dt} = \omega_t + \frac{3\gamma}{2\pi}\sum_{j\neq i}\frac{\mathbf{t}_i\cdot\mathbf{r}_{ij}\mathbf{r}_{ij}\cdot(\omega_n\mathbf{n}_j + \omega_t\mathbf{t}_j)}{|\mathbf{r}_{ij}|^5}, \qquad (1)$$

where $\mathbf{r}_{ij} = \mathbf{r}_i - \mathbf{r}_j$, $\omega_{t,n} = F_{t,n}/(\zeta b)$ are the reduced forces, and $\gamma = \zeta h^2/\eta = 6\pi a h^2$ is the hydrodynamic coupling constant. When the interaction is weak, we can simplify the phase equation [Eq. (1)] following a standard prescription [28]. To this end, we rewrite it in terms of the slow variable $\Phi_i = \phi_i - \omega_t t$, and then integrate it over a cycle under the approximation that Φ_i in the interaction term is constant over the period $2\pi/\omega_t$. We obtain

$$\frac{d\Phi_i}{dt} = -\frac{3\gamma\omega}{4\pi}\sum_{j\neq i}\frac{1}{|\mathbf{r}_{ij}|^3}\sin(\Phi_i - \Phi_j - \delta), \qquad (2)$$

where $\delta = \tan^{-1}(\omega_t/\omega_n)$ and $\omega = \sqrt{\omega_t^2 + \omega_n^2}$. This equation is correct to $O(\gamma/(d^3\sin\delta))$ [28,29]. In this form, the hydrodynamic coupling becomes isotropic, and our system resembles existing models of nonlocally coupled oscillators with phase delay [30,31].

Simulation method.—The model is implemented on a $L \times L$ square lattice with the grid size d, and the phase equation Eq. (1) is solved by Euler method with the time step Δt. The system size used is $L = 256$ for most of the results below, while we have also used $L = 128$ for obtaining some of the statistical data.

We have imposed periodic boundary condition and computed the velocity field at every time step by Fourier transformation. For $\delta > 0$, we also solved the reduced phase equation Eq. (2), to compare with the solution of Eq. (1), and found a very good agreement. We have also incorporated thermal fluctuations, by adding an uncorrelated Gaussian noise $\Omega_i(t)$ to the right-hand side of Eq. (1). The noise is assumed to have zero mean, and its fluctuations are controlled by the rotational diffusion constant of the bead $D_r = k_BT/(\zeta b^2)$ as $\langle\Omega_i(t)\Omega_j(t')\rangle = 2D_r\delta_{ij}\delta(t - t')$. We define the reduced (effective) temperature $\tau = \frac{D_r d^3}{\gamma\omega} = \frac{k_BTd^3}{36\pi^2\eta a^2b^2h^2\omega}$. For typical values of $a \sim b \sim h \sim 1\ \mu$m, $d \sim 10\ \mu$m, $\omega \sim 10^2$ Hz, with $\eta = 1\times 10^{-3}$ Pa s and $k_BT = 4\times 10^{-21}$ J, we have $\tau \sim 10^{-1}$. Note that the sharp dependence of τ on a, b, h, and d makes it easy to control the reduced temperature by changing the size or density of rotors. In our simulations, we have used the parameter values $\gamma = 0.1$ and $\omega = 0.1$, with $d = 1$ and $\Delta t = 0.1$. First, we turn off the thermal noise ($\tau = 0$) and vary the force angle δ to study the pattern dynamics.

Pumping-driven rotors.—When $\delta = 0$, each rotor pumps the fluid radially and is driven by the fluid flow generated by the other rotors. In this case, the initial random perturbations develop into topological defects (singularities of the phase field) $\phi(\mathbf{r})$ of winding numbers ± 1, which coarsen by collision of $+1$ and -1 defects and finally disappear to establish global synchronization.

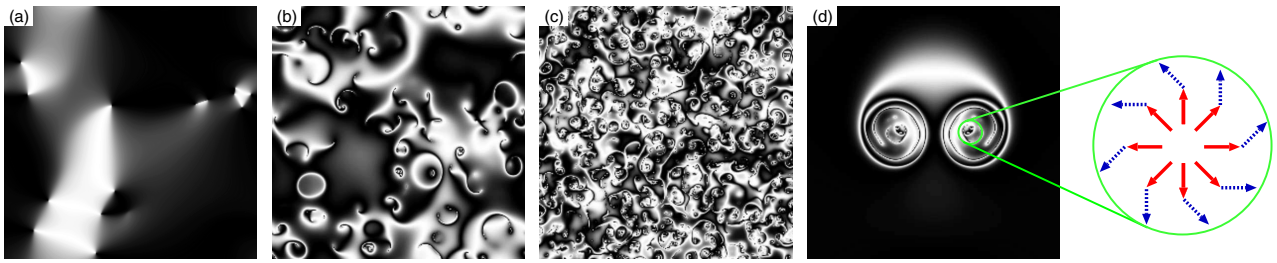

FIG. 2 (color online). Snapshots of coarsening defects (with the greyscale representing $\cos\phi(\mathbf{r})$) for (a) $\delta = 0$ and spiral waves for (b) $\delta = 45°$ and (c) $\delta = 60°$. These developed from random initial perturbations. (d) Spiral waves for $\delta = 60°$ evolving from a defect pair, with a schematic picture of the director field (red, solid arrows) and the velocity field (blue, dotted arrows) near a $+1$ defect.

Figure 2(a) shows a snapshot of the coarsening defects at $t = 10\,000$. To characterize the phase ordering dynamics, we define the correlation length $\xi = \langle[\nabla\phi(\mathbf{r})]^2\rangle_{\mathbf{r}}^{-1/2}$, where $\nabla\phi$ is the spatial gradient and $\langle\ldots\rangle_{\mathbf{r}}$ means spatial average. As shown in Fig. 3(a), we find that ξ as a function of time is well fitted by the power law $\xi \propto t^{\nu}$, with $\nu = 0.75$. The scaling of the hydrodynamic interaction $\mathbf{G}(\mathbf{r}) \sim |\mathbf{r}|^{-3}$ and Eq. (1) suggest that the characteristic time scale of a pattern is proportional to its size, which would mean $\nu = 1$. The difference between the numerical and scaling exponents suggests violation of dynamic scaling, which is characteristic to coarsening of point defects in two dimensions [32].

Torque-driven rotors.—When $\delta = 90°$, each rotor is driven by an active torque and exerts a force tangential to its orbit. In this case, we find that the system reaches a disordered state in which spatial correlation is almost completely lost. The absence of orientational correlation can be understood as follows. The average flow created by a rotor is perpendicular to its arm, and a neighboring rotor tends to align with the flow. Thus, the two rotors tend to be perpendicular to each other on average. However, it is not possible that every pair of rotors have their arms vertically crossed (geometric frustration), and hence the system evolves towards randomly oriented states.

Rotors driven by pumping and torque.—In the general case, the rotor is driven by an active torque while it pumps the fluid radially, and the total force exerted on the fluid has an angle $0° < \delta < 90°$ with respect to the arm of the rotor. We varied the parameter δ and found two types of dynamical behavior. For $0° < \delta \leq 40°$, the globally synchronized state is still obtained as the final state. However, for $40° < \delta < 90°$, we find that the dynamical steady state of the system involves self-proliferating spiral waves as shown in Figs. 2(b) and 2(c). Moreover, we find that the correlation length $\xi(t)$ converges to a finite value as $t \to \infty$ as shown in Fig. 3(a), and that the equilibrium correlation length decreases as δ is increased.

The flow pattern is locally correlated with the rotor's director $\mathbf{n}(\mathbf{r}) = (\cos\phi(\mathbf{r}), \sin\phi(\mathbf{r}))$. The surface flow velocity $\mathbf{v}(\mathbf{r})$ makes the angle δ with $\mathbf{n}(\mathbf{r})$ except at the core of the defect (see the movies [33] for comparison of the two fields). This observation leads us to an intuitive interpretation of the spiral waves. In the vicinity of a $+1$ defect from which the director emanates radially, the rotors create an outgoing flow that has an anticlockwise slant with respect to the radial direction, and hence form an anticlockwise spiral; see the inset of Fig. 2(d). The spiral is tighter for a larger force angle δ. We confirmed this scenario by choosing a defect pair as the initial configuration and following its evolution; see Fig. 2(d) and the corresponding movie [33]. Initially, clockwise and anticlockwise spirals are formed around -1 and $+1$ defects, respectively. Then, the director is randomized on the thinning spiral arm, which collapses and proliferates a cascade of new defects.

Thermal fluctuations.—We then introduce the thermal torque and study the phase behavior of the system. In Fig. 3(b), we plot the equilibrium order parameter $S = |\langle\cos\phi\rangle|$ as a function of the effective temperature. For $\delta = 0$, we find a critical temperature τ_c at which S vanishes as $S \propto \sqrt{\tau_c - \tau}$ to a good approximation [34]. We find the critical temperature for this phase transition as $\tau_c = 0.76$, which is about 30% smaller than the mean-field value $\tau_c = 1.08$ by Guirao and Joanny [4].

As we increase the phase delay δ up to $\delta_c = 40°$, the critical temperature is lowered down to $\tau_c = 0.61$. For $\delta > \delta_c$, the order parameter S is less than 1 even at $\tau = 0$ and is smaller for a larger system size L, suggesting that $S = 0$ in the thermodynamic limit. However, the existence of local order (spiral waves) is reflected in the finite-L data, using which we can define the transition temperature τ_c in the same way as mentioned before [34]. The resulting phase diagram is shown in Fig. 3(c). We distinguish three regions: (*O*) *ordered*, which is a distinct thermodynamic phase characterized by global synchronization, and (*S*) *spiral waves* and (*D*) *disordered*, which are inherently the same phase but with different local ordering and dynamical structure. Also shown in Fig. 3(c) are the contours of the correlation length ξ. While the *O*-*D* and *O*-*S* transitions are sharp, the *S*-*D* transition is a crossover characterized by gradual decrease of ξ. We also note that the

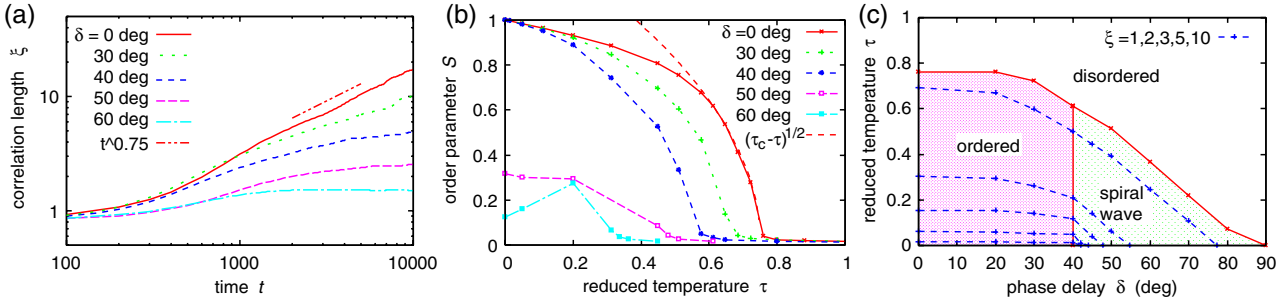

FIG. 3 (color online). (a) Correlation length ξ as a function of time and for different values of δ. For $\delta = 0°$, it is well fitted by $\xi \propto t^{0.75}$. For $\delta \leq \delta_c = 40°$, the correlation length diverges after $t = 10\,000$ (not shown), while for $\delta > \delta_c$, it remains finite. (b) Equilibrium order parameter S as a function of temperature τ and for different values of δ. (c) Phase diagram and contour of the correlation length ξ. The correlation length is smaller for larger δ and higher temperature.

frustrated state for $\delta = 90°$, $\tau = 0$, and the thermally disordered state for $\delta = 0°$, $\tau > \tau_c$ are qualitatively different, though they are not distinguished in the phase diagram.

Discussion.—The case of no active torque ($\delta = 0$) could be regarded as a simplified and idealized model of bacterial carpets [22,23]. Our model reproduced the enhancement of orientational ordering, while it predicts global ordering and not the finite-size correlation as observed in the experiments. The experimental patterns might be explained by some kind of frozen disorder in the flagellar configuration, which can be readily incorporated in our model [29,35]. The case of $\delta = 90°$ is realized by rigid spheres without pumping. It is related to a recently studied model of two rigid spheres making tilted elliptic orbits [17], which show both in-phase and antiphase synchronization. Our results suggest that the interaction between many of such rotors is frustrated, and the system does not attain full synchronization. Spiral waves for finite phase delay δ have been observed in previous models of 2D coupled oscillators [30,31,36]. However, in our case, the pattern is intrinsically turbulent and self-proliferating, in contrast to the case of finite-range coupling, for which the phase is spatially smooth except near the defect core [30,31,36].

In conclusion, we have introduced a generic model of microfluidic rotors that shows a variety of dynamical patterns including global synchronization, fully disordered states, and self-proliferating spiral waves. The patterns are sensitively controlled by the angle of active force δ (the degree of frustration) and the temperature τ. Our results suggest that arrays of active microfluidic components could be designed to induce a rich variety of dynamical behaviors in the vicinal fluid, and could be used to make switchable microfluidic mixers.

N. U. thanks the hospitality at University of Sheffield where this work was initiated, and financial support from Grant-in-Aid for Scientific Research from MEXT. R. G. acknowledges financial support from the EPSRC.

*uchida@cmpt.phys.tohoku.ac.jp
†r.golestanian@sheffield.ac.uk

[1] E. M. Purcell, Am. J. Phys. **45**, 3 (1977).
[2] I. H. Riedel, K. Kruse, and J. Howard, Science **309**, 300 (2005).
[3] S. Gueron and K. Levit-Gurevich, Proc. Natl. Acad. Sci. U.S.A. **96**, 12240 (1999).
[4] B. Guirao and J-F. Joanny, Biophys. J. **92**, 1900 (2007).
[5] J. Elgeti, Ph.D. thesis, Universität zu Köln, 2007.
[6] K. Drescher *et al.*, Phys. Rev. Lett. **102**, 168101 (2009).
[7] J. L. McWhirter, H. Noguchi, and G. Gompper, Proc. Natl. Acad. Sci. U.S.A. **106**, 6039 (2009).
[8] T. J. Pedley and J. O. Kessler, Annu. Rev. Fluid Mech. **24**, 313 (1992).
[9] R. A. Simha and S. Ramaswamy, Phys. Rev. Lett. **89**, 058101 (2002); Y. Hatwalne *et al.*, Phys. Rev. Lett. **92**, 118101 (2004); A. Ahmadi, M. C. Marchetti, and T. B. Liverpool, Phys. Rev. E **74**, 061913 (2006).
[10] D. Saintillan and M. J. Shelley, Phys. Rev. Lett. **100**, 178103 (2008).
[11] J. P. Hernandez-Ortiz, C. G. Stoltz, and M. D. Graham , Phys. Rev. Lett. **95**, 204501 (2005); T. Ishikawa and T. J. Pedley, J. Fluid Mech. **588**, 437 (2007); I. S. Aranson *et al.*, Phys. Rev. E **75**, 040901(R) (2007).
[12] C. M. Pooley, G. P. Alexander, and J. M. Yeomans , Phys. Rev. Lett. **99**, 228103 (2007).
[13] G. P. Alexander and J. M. Yeomans, Europhys. Lett. **83**, 34006 (2008).
[14] E. Lauga and D. Bartolo, Phys. Rev. E **78**, 030901(R) (2008).
[15] M. Kim *et al.*, Proc. Natl. Acad. Sci. U.S.A. **100**, 15481 (2003); M. Kim and T. R. Powers, Phys. Rev. E **69**, 061910 (2004); B. Qian *et al.*, arXiv:0904.2347.
[16] M. Reichert and H. Stark, Eur. Phys. J. E **17**, 493 (2005).
[17] A. Vilfan and F. Jülicher, Phys. Rev. Lett. **96**, 058102 (2006).
[18] M. C. Lagomarsino, P. Jona, and B. Bassetti, Eur. Phys. J. B **26**, 81 (2002); Phys. Rev. E **68**, 021908 (2003).
[19] Y. W. Kim and R. R. Netz, Phys. Rev. Lett. **96**, 158101 (2006).
[20] R. E. Goldstein, M. Polin, and I. Tuval, Phys. Rev. Lett. **103**, 168103 (2009).
[21] V. B. Putz and J. M. Yeomans, J. Stat. Phys. **137**, 1001 (2009).
[22] N. Darnton *et al.*, Biophys. J. **86**, 1863 (2004).
[23] M. J. Kim and K. S. Breuer, J. Fluids Eng. **129**, 319 (2007); Small **4**, 111 (2008).
[24] R. Dreyfus *et al.*, Nature (London) **437**, 862 (2005); P. Tierno *et al.*, Phys. Rev. Lett. **101**, 218304 (2008).
[25] R. A. van Delden *et al.*, Nature (London) **437**, 1337 (2005); J. Vicario *et al.*, Nature (London) **440**, 163 (2006).
[26] R. Dreyfus, J. Baudry, and H. A. Stone, Eur. Phys. J. B **47**, 161 (2005).
[27] J. R. Blake, Proc. Cambridge Philos. Soc. **70**, 303 (1971).
[28] Y. Kuramoto, *Chemical Oscillations, Waves, and Turbulence* (Springer, New York, 1984).
[29] N. Uchida and R. Golestanian (to be published).
[30] S. Shima and Y. Kuramoto, Phys. Rev. E **69**, 036213 (2004).
[31] P-J. Kim *et al.*, Phys. Rev. E **70**, 065201(R) (2004).
[32] R. E. Blundell and A. J. Bray, Phys. Rev. E **49**, 4925 (1994).
[33] See supplementary material at http://link.aps.org/supplemental/10.1103/PhysRevLett.104.178103 for movies showing the evolution of the system for the different cases shown in Fig. 2.
[34] In practice, S remains finite even for $\tau > \tau_c$ due to the finite-size effect; we defined τ_c by $S(\tau_c) = 2S_0$ where S_0 is the theoretical value of S for a noninteracting ($\gamma = 0$) system.
[35] N. Uchida and R. Golestanian, Europhys. Lett. **89**, 50011 (2010).
[36] H. Sakaguchi, S. Shinomoto, and Y. Kuramoto, Prog. Theor. Phys. **79**, 1069 (1988); J. E. Paullet and G. B. Ermentrout, SIAM J. Appl. Math. **54**, 1720 (1994).